HHS Public Access

Author manuscript

Mol Cancer Res. Author manuscript; available in PMC 2020 March 01.

Published in final edited form as:

Mol Cancer Res. 2019 September ; 17(9): 1893–1909. doi:10.1158/1541-7786.MCR-18-1191.

Cigarette Smoke Induces Metabolic Reprogramming of the Tumor Stroma in Head and Neck Squamous Cell Carcinoma

Marina Domingo-Vidal[1], **Diana Whitaker-Menezes**[1], **Cristina Martos-Rus**[1], **Patrick Tassone**[2], **Christopher M. Snyder**[3], **Madalina Tuluc**[4], **Nancy Philp**[4], **Joseph Curry**[2,*], **Ubaldo Martinez-Outschoorn**[1,*]

[1]Department of Medical Oncology, Sidney Kimmel Cancer Center, Thomas Jefferson University – Philadelphia, PA

[2]Department of Otolaryngology – Head and Neck Surgery, Thomas Jefferson University – Philadelphia, PA

[3]Department of Microbiology and Immunology, Sidney Kimmel Cancer Center, Thomas Jefferson University – Philadelphia, PA

[4]Department of Pathology, Anatomy and Cell Biology, Sidney Kimmel Cancer Center, Thomas Jefferson University – Philadelphia, PA

Abstract

Head and neck squamous cell carcinoma (HNSCC) is comprised of metabolically linked distinct compartments. Cancer-associated fibroblasts (CAFs) and non-proliferative carcinoma cells display a glycolytic metabolism, whilst proliferative carcinoma cells rely on mitochondrial oxidative metabolism fueled by the catabolites provided by the adjacent CAFs. Metabolic coupling between these reprogrammed compartments contributes to HNSCC aggressiveness. In the current study, we examined the effects of cigarette smoke-exposed CAFs on metabolic coupling and tumor aggressiveness of HNSCC. Cigarette smoke (CS) extract was generated by dissolving cigarette smoke in growth media. Fibroblasts were cultured in CS or control media. HNSCC cells were co-cultured in vitro and co-injected in vivo with CS- or control fibroblasts. We found that CS induced oxidative stress, glycolytic flux and MCT4 expression, and senescence in fibroblasts. MCT4 upregulation was critical for fibroblast viability under CS conditions. The effects of CS on fibroblasts were abrogated by antioxidant treatment. Co-culture of carcinoma cells with CS-fibroblasts induced metabolic coupling with upregulation of the marker of glycolysis MCT4 in fibroblasts and markers of mitochondrial metabolism MCT1 and TOMM20 in carcinoma cells. CS-fibroblasts increased CCL2 expression and macrophage migration. Co-culture with CS-fibroblasts also increased two features of carcinoma cell aggressiveness: resistance to cell death and enhanced cell migration. Co-injection of carcinoma cells with CS-fibroblasts generated larger tumors with reduced apoptosis than control co-injections, and upregulation of MCT4 by CS

[*]Corresponding Authors: Joseph Curry, MD, Sidney Kimmel Cancer Center Dept of Otolaryngology, 925 Chestnut Street, Suite 740, Philadelphia PA 19107, joseph.curry@jefferson.edu, Ubaldo Martinez-Outschoorn, MD, Sidney Kimmel Cancer Center Dept of Medical Oncology, 233 S 10th Street, Suite 909, Philadelphia, PA 19107, ubaldo.martinez-outschoorn@jefferson.edu.

Conflict of Interest: None

exposure was a driver of these effects. We demonstrate that a tumor microenvironment exposed to CS is sufficient to modulate metabolism and cancer aggressiveness in HNSCC.

Introduction

Head and neck cancer is the 6th most common type of cancer worldwide, with an incidence of 600,000 new cases every year[1]. Head and neck squamous cell carcinoma (HNSCC) accounts for nearly 95% of head and neck malignancies. Cigarette smoke (CS) is the major causative agent of HNSCC. Smokers are at much higher risk to develop the disease than non-smokers, as well as being more likely to have worse treatment outcomes and shorter disease survival[2, 3]. CS contains over 70 known carcinogens[4]. DNA damage and adduct formation is thought to be the common mechanism by which these compounds cause mutations and drive carcinogenic transformation of the epithelial cells in the head and neck region[4]. However, the effects of CS on the stromal cells within the tumor microenvironment of HNSCC has not been explored in detail.

The tumor stroma plays an important role in HNSCC development and progression, and there is increasing interest in the metabolic interplay between cancer cells and the surrounding non-cancerous cells[5–8]. Two studies from Curry *et al* show that at least two metabolically distinct compartments exist within the tumor microenvironment of HNSCC[9, 10]. The tumor stroma, which contains abundant cancer-associated fibroblasts (CAFs), is highly glycolytic and secretes high-energy catabolites such as lactate and pyruvate. The proliferating carcinoma cells take advantage of this metabolic compartmentalization since they are mitochondria-rich and utilize these catabolites to fuel their oxidative metabolism. Markers of metabolic compartmentalization have been described in HNSCC and are associated with aggressive disease[5, 9]. The monocarboxylate transporter 4 (MCT4), which is an exporter of lactate and has a hypoxia response element regulated by HIF1α, is a marker of glycolysis in CAFs. The importer of monocarboxylates MCT1 and the translocase of the outer mitochondrial membrane 20 (TOMM20) are markers of lactate intracellular uptake and high mitochondrial oxidative phosphorylation (OXPHOS) in carcinoma cells. Studying the metabolic compartmentalization of tumors is important not only to understand the pathophysiology of cancer but also to develop therapeutic targets. For instance, it has been recently demonstrated that the antidiabetic drug metformin, a mitochondrial inhibitor, affects tumor metabolic compartmentalization and has anticancer effects in HNSCC[11, 12].

Research on the pathogenesis of smoking-related diseases such as pulmonary emphysema and lung cancer has prompted the study of the effects of CS on tissue fibroblasts. It has been demonstrated that exposure of lung fibroblasts to CS induces oxidative stress, cellular senescence and apoptosis, as well as inhibits proliferation, migration, and extracellular matrix deposition[13–15]. Some of these effects have also been reported in human gingival and skin fibroblasts exposed to CS[16–19]. Numerous studies have also shown that CS induces pro-inflammatory signaling cascades and chemokine secretion in fibroblasts[20–22], creating a chronic inflammatory state that may contribute to the development and progression of cancer. The mechanisms by which CS elicits its effects on fibroblasts include generation of

intracellular reactive oxygen species (ROS) with alteration in the cellular redox state. In fact, treatment with antioxidants such as N-acetylcysteine (NAC) or overexpression of endogenous antioxidant systems protects fibroblasts from CS-induced ROS and cellular damage[13, 23–25]. Moreover, signaling through the aryl hydrocarbon receptor (AhR), a regulator of the inflammatory response, attenuates oxidative stress, and reduces apoptosis and inflammation triggered by CS in lung fibroblasts[26–29].

While the effect of CS on isolated fibroblasts has been studied, very little is known about how these altered fibroblasts affect the microenvironment and epithelial cells in proximity. To our knowledge, only two reports have shown the effects of CS on fibroblasts in the context of cancer[19, 30]. Salem *et al* demonstrated in breast cancer that CS-exposed fibroblasts have the ability to metabolically promote tumor growth in a paracrine fashion, thus highlighting the importance of the stromal compartment in tumors[19]. Studies of the effect of cigarette smoke on HNSCC stroma, however, have not been published. Therefore, we aimed to study the effects of CS exposure to fibroblasts on HNSCC metabolic compartmentalization, oxidative stress, inflammation and aggressiveness.

Materials and Methods

Preparation of Cigarette Smoke Extract

Cigarette smoke extract (CSE) was generated as described by attaching one end of a three-way-stopcock to a 60 mL syringe containing 10 mL of un-supplemented DMEM medium, and another end to a Marlboro Red cigarette (Philip Morris, Richmond, VA) (Suppl. Fig. 1A)[13, 19, 31–34]. Briefly, 40 mL of cigarette smoke was pulled through the stopcock into the syringe and dissolved in the media by vigorous shaking. The cigarette was “smoked” down to the filter, approximately 7–8 puffs for one cigarette. The 10 mL of media with contents of one cigarette was treated as 100% CSE stock. This stock was diluted to 5% CSE in DMEM media, supplemented with 10% FBS and Penicillin-Streptomycin (Pen-Strep), and sterile filtered through a 0.22 μm filter.

Cell culture

The human tongue and hypopharynx squamous cell carcinoma cell lines, CAL27 and FaDu, respectively, were purchased from ATCC. The human papilloma virus (HPV+)-transformed mouse tonsil epithelial cell, MTEC, from male C57Bl/6 mice was a kind gift from Dr. Ulrich Rodeck. Human skin fibroblasts immortalized with human telomerase reverse transcriptase catalytic domain (BJ1) were purchased from Clontech, and clones were generated with green fluorescent protein (GFP). The BALB/c mouse monocyte/macrophage cell line, RAW 264.7, was a kind gift from Dr. Craig Hooper. All cell lines were obtained from cell banks and authenticated by short tandem repeat (STR) DNA analyses prior to receipt by our laboratory. These cells were passaged in our laboratory for fewer than 8 weeks after resuscitation. All cells were tested for mycoplasma using the Universal Mycoplasma Detection Kit (30–1012K; ATCC) and were negative for myocoplasma within 2 months of cell thawing and experimental work. Cells were cultured in DMEM (10566016; Gibco) supplemented with 10% heat inactivated fetal bovine serum (FBS) (161407–071; Gibco),

100 units/ml penicillin, and 100 units/ml streptomycin (Pen-Strep; 30–002-CI; Corning). Cell cultures were maintained in a 37°C and 5% CO_2 humidified incubator.

Isolation of Mouse Embryonic Fibroblasts

Mouse Embryonic Fibroblasts (MEFs) were isolated from genetically engineered C57BL/6 mice lacking MCT4 (MCT4 −/−) and their wild-type control (MCT4 +/+) (provided by Dr. Nancy Philp[36]). Pregnant female mice were euthanized at E14.5 by CO_2 inhalation. Under sterile conditions, the abdominal wall was exposed and the uterus was removed and transferred to a Petri dish containing PBS and pen-strep. Embryos were separated from the placenta and placed into a new dish with PBS for individual manipulation. Head, arms, and legs were cut off, and internal red tissue (heart and liver) was removed. The remaining embryo was minced, transferred to a tube containing 0.25% trypsin-EDTA, incubated for 10 minutes at 37°C, and then MEF culture media (DMEM 10% FBS) was added to the tube. Cell suspension was left for 5 minutes to allow large fragments to precipitate and supernatant was transferred to 10 cm Petri dishes. Media was replaced once MEFs were seen attached to the plate. MEFs were maintained in DMEM 10% FBS Pen Strep for no longer than ten passages.

Cell treatments

BJ1 fibroblasts were plated in 12- or 6-well plates or 10 cm dishes with standard growth media (CTRL-BJ1) or 5% CSE media (CSE-BJ1), as indicated. The seeding densities were 10×10^4 cells/well (for 12-well), 20×10^4 cells/well (for 6-well) and 10^6 cells/dish. Control media or 5% CSE was replaced every two days, for a total of 4 or 6 days. Fresh CSE was generated for each use. When indicated, 30 μg/ml of liposomal glutathione, 50 or 100 μM of L-kynurenine (L-KYN, K8625; Sigma), 5 or 10 μM of α-naphthoflavone (α-NF, N5757; Sigma), or the vehicle DMSO, were added to CTRL- and CSE-BJ1 at time of seeding and every time media was replaced, for a total of 4 days. WT and MCT4-KO MEFs were plated in 6- or 12-well plates, or T-75 flasks with standard growth media, at a density of 10×10^4 or 20×10^4 cells/well, or 2×10^6 cells/flask, respectively. The following day, MEFs were treated with either 5% or 10% CSE or control media, with or without 30 μg/ml liposomal glutathione, as indicated, for 24 hours. RAW 264.7 cells were plated in 6-well plates with standard growth media at a density of 6×10^5 cells/well. The following day, RAW 264.7 were treated with 5% CSE or control media for 24 hours.

Co-culture system

CAL27 and FaDu human carcinoma cells were co-cultured with either CTRL- or CSE-BJ1 (Suppl. Fig. 1B) in 12- or 6-well plates or 10 cm dishes, as specified. All co-cultures were seeded at a 5:1 fibroblast-to-carcinoma ratio in standard DMEM media. The total number of cells per well was 1×10^5 (12-well), 2.4×10^5 (6-well), and per dish was 12×10^5. MTEC mouse carcinoma cells were co-cultured with WT MEFs, untreated or previously exposed to 5% CSE. 6×10^4 MTEC cells were cultured at the bottom of a 6-well plate, and 20×10^4 MEFs were cultured on top of a polycarbonate cell culture insert with a 0.4 μm pore-size membrane (353090; Thermo Fisher). The following day, culture media was changed to DMEM with 10% Nu-serum, a low protein alternative to FBS (355100; BD Biosciences) containing Penicillin-Streptomycin. Co-cultures were maintained in this media for 3 days.

Immunofluorescence

Immunofluorescence staining from cells in 12-well plates was performed as previously described[35]. Primary antibodies used included anti-MCT4 (19-mer peptide sequence CKAEPEKNGEVVHTPETSV-cooh affinity purified rabbit antibody; YenZym Antibodies), anti-GLB1 (ab96239; Abcam), anti-HMGB1 (NB100–2322; Novus Biologicals), and anti-MCT1 (19-mer peptide sequence CSPDQKDTEGGPKEEESPV-cooh affinity purified rabbit antibody; YenZym). Anti-rabbit AlexaFluor 568 (A11036; Invitrogen) secondary antibody was used. Nuclear counterstaining was performed with DAPI. Images were collected with a 40x objective and 1.5 or 2x zoom, when indicated, using a Nikon A1R confocal microscope.

Immunoblotting

Protein lysates were obtained from CTRL- and CSE-BJ1 cultured in 10 cm dishes. Protein extraction, quantification and immunoblotting were performed as described previously[19]. Primary antibodies used included anti-MCT4 (sc-50329; Santa Cruz), anti-GLB1 (ab96239; Abcam), anti-HMGB1 (NB100–2322; Novus Biologicals), anti-NF-κB (3033; Cell Signaling), anti-pRB (9308; Cell Signaling), anti-TIGAR (ab37910; Abcam), anti-β-actin (A5441; Sigma-Aldrich), anti-β-tubulin (T4026; Sigma-Aldrich), and anti-vinculin (#4650; Cell Signaling).

Lactate Assay

After 4 days in standard growth media or 5% CSE, with or without 30 μg/ml of glutathione, media from BJ1 fibroblasts cultured in 12-well plates was replaced by 400 μl of phenol-free DMEM 10% FBS. After 16 hours, cell media was collected and L-lactate levels were assessed according to the manufacturer's instructions using the EnzyChromTM L-Lactate Assay Kit (ECLC-100; BioAssay Systems). Results were normalized for total cell number.

Reactive Oxygen Species Assay

After 4 days in standard growth media or 5% CSE, with or without 30 μg/ml of glutathione, media from BJ1 fibroblasts cultured in 12-well plates was replaced by DMEM 10% FBS containing 5 μM CellROX™ Deep Red reagent (C10422; Invitrogen). After 30 min incubation at 37°C, BJ1 were harvested and CellROX fluorescence was detected by flow cytometry using an APC signal detector. Analysis was performed with FlowJo software.

Cell viability assessment

BJ1 fibroblasts were washed twice with PBS and fixed with 4% paraformaldehyde (PFA) for 10 min at room temperature. Fixed cells were then rinsed with PBS and stained with 0.5% crystal violet (CV, C0775; Sigma) in 10% ethanol. CV was removed and cells were washed with deionized water. Cells were left to dry and then photographed under an inverted phase microscope.

Flow cytometry assessment of metabolic markers

After 4 days of co-culture in 6-well plates, cells were collected and subject to immunostaining and flow cytometry analysis, as previously described[11]. Primary antibodies used were anti-MCT1 (YenZym), anti-TOMM20 (sc-17764; Santa Cruz), and anti-MCT4

(YenZym). Secondary antibodies used were anti-rabbit and anti-mouse conjugated to an APC or PE fluorophore, as indicated. Cell populations were separated by GFP detection when indicated.

Apoptosis and Cell Death Assessment

After 4 days of co-culture in 12-well plates, the culture media and cells were collected, centrifuged, and re-suspended in Annexin-V (AnnV) binding buffer containing Ann-V-APC conjugate (550474; BD Biosciences) and propidium iodide (PI) (KPL 71-04-01; SeraCare). Populations of cells were separated by GFP detection. AnnV and PI staining were assessed by flow cytometry and analysis was performed with FlowJo software. The same protocol was followed on monocultures of WT and MCT4-KO MEFs treated with or without CSE and GSH for 2 days. Quadruplicates were run for each condition.

Transwell Migration Assay

24-well polycarbonate plates with 6.5 mm diameter inserts and 8 μm-pore-sized membranes (3422; Costar) were used to study the migratory capabilities of carcinoma cells and macrophages. 5×10^5 CAL27 or FaDu cells, or 10^6 RAW 264.7 cells were added to the top of the insert, and 1×10^5 CTRL- and CSE-BJ1 or 15×10^4 MEF were seeded in the lower chamber, all in 10% Nu-serum DMEM media. Cells were allowed to migrate for 24 hours and membranes were stained with crystal violet. Images were then taken under an inverted phase microscope and staining was quantified with ImageJ.

Analysis of CCL2 mRNA levels

Total RNA from WT and MCT4-KO MEFs exposed to CTRL- or 5% CSE-media was isolated using TRIzol® Reagent (15596026; Invitrogen) following manufacturer's instructions. Total RNA concentration and purity was determined using NanoDrop® ND-1000 spectrophotometer (Thermo Scientific). Reverse transcription polymerase chain reaction (RT-PCR) was performed using a High-Capacity cDNA Reverse Transcription Kit (4368814; Applied Biosystems) and carried out in a Bio-Rad PTC-100® thermal cycler. cDNA obtained was used to perform real-time PCR target amplification. Quantitative Polymerase Chain Reaction (qPCR) master mixes were prepared using TaqMan Universal PCR Master Mix (4304437; Applied Biosystems) according to manufacturer's recommendations and loaded into MicroAmp® Optical 384-Well reaction plates (4483319; Applied Biosystems). Inventoried TaqMan® Gene expression assays CCL2 (Mm00441242_m1), β-actin (Mm00607939_s1) and GAPDH (Mm00607939_s1) were used. Each qPCR reaction was performed in triplicates. Plates were analyzed in a QuantStudio 12K Flex Real-Time PCR System (Thermo Scientific). mRNA expression levels were calculated using the relative comparison CT ($2\text{-}\Delta\Delta CT$) method after normalization with GAPDH as endogenous control.

Immunohistochemistry (IHC)

Excised tumors were frozen with liquid nitrogen in Tissue Tek O.C.T. (4583; Electron Microscopy Sciences) and sectioned at 6 μm thickness. Sections were fixed with 4% PFA in PBS for 10 min at room temperature, washed with PBS, and blocked with 5% BSA/PBS for

30 min. Endogenous biotin activity was blocked using the Avidin-Biotin Kit (AB972 L; Biocare Medical), and endogenous peroxidase activity with 0.3% H_2O_2 0.3% Na Azide in PBS for 15 min. Primary antibodies anti-CD45 (550539; BD Biosciences) and anti-CD68 (137001; Biolegend) were incubated for 1 hour at room temperature. Biotinylated anti-rat secondary antibody (BA-4001; Vector Laboratories), and avidin-horseradish peroxidase complex (Vectastain Elite ABC kit, PK-6100; Vector Laboratories) were each incubated for 30 min. Antibody reactivity was detected using liquid DAB substrate chromagen (K346711–2; Agilent) and counterstaining of nuclei was performed with Tacha's hematoxylin (NH-HEM M; Biocare Medical). Representative images were taken at a 20X magnification and quantified by ImageJ.

Quantification with ImageJ

CD45 and CD68 by IHC and crystal violet (CV) staining were quantified with ImageJ. RGB images were first split into single color channels with the "RGB stack" tool. Staining was highlighted using the "threshold" tool. Thresholds were adjusted to select all stained areas and the same values were maintained across all images for comparison. The "measure" tool calculated the % of stained area relative to the total area of the region of interest (ROI), which was the same for all images.

TUNEL Assay and Quantification of Apoptotic Cells in Tumors

Frozen sections were fixed with 4% paraformaldehyde in PBS for 10 min, washed with PBS and permeabilized with 30% acetic acid in 100% ethanol at −20C for 5 min. After washing, sections were incubated with equilibration buffer (S7106; Millipore-Sigma) for 15 min at room temperature (RT) and then with ApopTag TdT enzyme (S7107; Millipore-Sigma) and reaction buffer (S7105; Millipore-Sigma) at a ratio of 30:70 for 30 min at 37C. Sections were washed in PBS and incubated with anti-digoxigenin-POD (11207733910; Sigma) for 30 min at RT. TUNEL positive cells were visualized with liquid DAB substrate kit (Agilent).

Apoptotic nuclei were quantified using Aperio software (Aperio, Nussloch, Germany). Digital images were captured with Leica and Aperio slide scanners under 320 magnification with an average scan time of 120 seconds (compression quality 70). A nuclear algorithm was used to identify TUNEL positive cells and generate values for percentage of 3+ nuclei. Four tumors from each group were evaluated. In the CAL27 xenografts, 9–11 areas of tumor cells were analyzed for each xenograft and quantified for a total of 38 areas in the control and 40 areas in CSE-treated For the FaDu xenografts, 10–15 areas of tumor cells were analyzed for each xenograft and quantified for a total of 50 areas in the control and 51 areas in CSE-treated.

Animal studies

All animal work was approved by the Institutional Animal Care and Use Committee (IACUC) at Thomas Jefferson University. Male athymic nude mice aged 4–6 weeks (Charles River) were maintained under standard pathogen-free conditions in our animal facility. Animals were provided with sterilized chow and water. All animal handling and experiments were conducted under the standards of the IACUC.

CAL27, FaDu, CTRL-BJ1, and CSE-BJ1 cells were cultured in parallel, then trypsinized and resuspended in PBS (Suppl. Fig. 1B). 3×10^5 CAL27 or FaDu carcinoma cells were co-injected with 10^6 CTRL- or CSE-BJ1 fibroblasts bilaterally into the flanks of nude mice. Each group contained five mice and a total of 10 tumor xenografts. As controls, five mice were also injected with 10^6 CTRL- or CSE-BJ1 alone. Starting on day 14, tumors were measured twice weekly with an electronic caliper. Mouse weight was also monitored biweekly. Mice were sacrificed and tumors harvested at post-injection days 13 (CAL27) or 21 (FaDu) as an early time-point, and day 24 as the end-point. Excised tumor measurements were taken by electronic caliper. Tumor volume (mm^3) was calculated by the formula $v = (x^2y/2)$, where v is the volume of the tumor, x is the length of the short axis, and y is the length of the long axis.

Male C57Bl/6 mice were purchased from Taconic Farms. 10^5 MTEC cells were co-injected with 10^6 WT-MEF or MCT4-KO MEF bilaterally in the flank. Two different sets of co-injections were performed at different times: co-injections with CSE-unexposed WT and MCT4-KO MEFs (control MEFs) and co-injections with CSE-treated WT and MCT4-KO MEFs (CSE MEFs). Both sets were allowed to grow for a period of 28 days. Tumor volume and weight were measured at the time of collection.

Human study

This study was approved by the institutional review board (IRB) at Thomas Jefferson University. Samples of primary tumors from 36 patients with head and neck cancer were obtained from archived paraffin-embedded tissue blocks for histological analysis. Patient data were collected including: age, sex, tobacco use, HPV status, tumor primary site and subsite.

MCT4 Immunohistochemistry and Analyses in Head and Neck Cancer Samples

Paraffin sections were deparaffinized, rehydrated and antigen retrieval was performed in 0.01M Tris-EDTA, pH 9.0 with 0.1% Tween-20 for 10 minutes using a pressure cooker. The sections were blocked with 3% H_2O_2 and for endogenous biotin; then incubated with 10% goat serum (Vector) at 4°C overnight. MCT4 antibody (sc-376140; Santa Cruz Biotechnology) was applied for one hour, followed by biotinylated secondary antibody and avidin-biotin-HRP complex. A DAB liquid substrate kit was used to detect binding and slides were stained with hematoxylin and mounted.

MCT4 staining was evaluated in a blinded fashion by two independent observers. Multiple fields for each slide were viewed at low and high power and an overall score of either ≤50% or >50% staining in cancer-associated stroma was determined. Samples with disparate scores were reviewed and a score was jointly determined. For immune-rich versus immune-poor status, MCT4 and H&E stained slides were evaluated in a similar fashion. The samples were labeled as having an immune-rich stroma if greater than 50% of the stromal cells were immune cells. Samples with disparate scores were reviewed jointly and in addition by an expert pathologist (MT).

Statistical Analysis

Statistical significance was examined using the Student's t-test and Fisher's exact text. Differences were considered statistically significant at $p<0.05$.

Results

Cigarette Smoke Extract induces senescence and glycolysis in fibroblasts

To examine the effects of CSE exposure on the metabolism and stress response mechanisms of BJ1 human skin fibroblasts, cells were exposed to 5% CSE (CSE-BJ1) or standard media (CTRL-BJ1) for 6 days. After CSE exposure, changes in BJ1 proliferation and cell morphology were observed. Compared to untreated cells, CSE-BJ1 were less confluent and cells were enlarged (Fig. 1A), which are two features of cellular senescence. Decreased proliferation rates of CSE-BJ1 were consistent with decreased expression of phosphorylated retinoblastoma protein (p-RB), an inducer of cell cycle progression. CSE-BJ1 had decreased pRB, which prevents G1 progression through the cell cycle, compared to CTRL-BJ1 (Fig. 1B). CSE-BJ1 were also more senescent and showed increased β-galactosidase expression and loss of nuclear HMGB1 (note intranuclear dots) compared to CTRL-BJ1 by immunofluorescence (Fig. 1C) and western blot (Fig. 1D). In terms of metabolism, CSE-BJ1 had increased MCT4 expression compared to CTRL-BJ1 (Fig. 1E, F), indicating a switch towards a glycolytic metabolism. To confirm the increased glycolytic flux in CSE-BJ1, we determined the levels of lactate secretion, which is the end-product of glycolysis, and intracellular ROS levels, which is a driver of MCT4 expression. CSE-BJ1 increased lactate secretion compared to controls (Fig. 1G), consistent with an augmented glycolytic metabolism of fibroblasts upon CSE exposure. Intracellular ROS levels were also increased in CSE-BJ1 (Fig. 1H), correlating with the upregulation of MCT4 expression.

α-naphthoflavone mimics the effects of CSE on fibroblasts

Since CSE induces ROS generation and increases MCT4 expression in our model, we investigated whether the aryl hydrocarbon receptor (AhR), which is involved in compensatory responses to inflammation and oxidative stress, was able to regulate MCT4 expression. We pharmacologically modulated the AhR in unexposed BJ1 fibroblasts and assessed MCT4 and NF-κB expression, to determine the inflammatory state of the cell. Treatment of BJ1 fibroblasts with the AhR agonist L-kynurenine (L-KYN) decreased the expression of both p65 subunit of NF-KB and MCT4 (Fig. 2A, B). Conversely, the AhR antagonist α-naphthoflavone (α-NF) triggered a dose-dependent upregulation of both p65 subunit of NF-kB and MCT4 expression (Fig. 2C, D). This data in BJ1 fibroblasts is consistent with the known anti-inflammatory role of the AhR and suggests that the AhR signaling pathway regulates ROS scavenging and, consequently, the levels of MCT4. To determine whether these modulators of the AhR have effects on CSE-exposed fibroblasts, BJ1 cells were treated with 5% CSE or control media, containing increasing concentrations of L-KYN or α-NF, and apoptosis and cell death rates were quantified. As expected, CSE-cultured fibroblasts, regardless of drug treatment, presented higher apoptosis and cell death rates than fibroblasts cultured in control media (Fig. 2E, F). L-KYN had no effects on fibroblast viability in either CTRL- or CSE-BJ1 (Fig 2E). α-NF did not mimic the effects of the CSE on CTRL-BJ1, however it increased cell death and apoptosis in CSE-BJ1 in a dose-

dependent manner (Fig 2F). This suggests that the anti-inflammatory effects derived from the AhR agonist L-KYN are not sufficient to protect fibroblasts from the CSE, whereas antagonizing the AhR signaling with α-NF has an additive effect to the detrimental effect of the CSE on fibroblasts.

The antioxidant glutathione abrogates the effects of CSE

As ROS seem to be driving the effects of CSE on fibroblasts, we next aimed to assess the effects of the antioxidant glutathione (GSH) on cell viability, ROS levels, MCT4 expression, and lactate efflux in our model. Treatment with GSH improved the viability of CSE-exposed fibroblasts, as seen by crystal violet staining (Fig. 3A). Regarding ROS levels, CSE-BJ1 have greatly increased intracellular ROS levels compared to CTRL-BJ1 (Fig. 3B, left). GSH treatment reduces ROS levels by 80% (Fig. 3B, right). MCT4 expression, quantified by flow cytometry, followed the same trend as ROS levels. CSE-BJ1 not treated with GSH increased MCT4 levels by almost 3-fold respect to CTRL-BJ1 (Fig. 3C, left), whereas addition of the antioxidant attenuated this response to 1.8-fold (Fig. 3C, right). The decrease in MCT4 expression observed in the GSH treated cells was accompanied by a decrease in lactate levels in media of CSE-BJ1 (Fig. 3D). The antioxidant N-acetylcysteine (NAC), precursor of glutathione, elicits the same effects as GSH in terms of increasing cell viability (Suppl. Fig. 2A) and reversing MCT4 expression (Suppl. Fig. 2B) upon CSE exposure. Moreover, NAC reverses the effects of CSE on the expression of the TP53-induced glycolysis and apoptosis regulator (TIGAR) protein, which is involved in the antioxidant defense and apoptosis suppression (Suppl. Fig. 2C). This data suggests that fibroblasts increase MCT4 expression and lactate production in response to elevated ROS levels induced by the CSE treatment.

To examine whether the increase in MCT4 expression was linked to viability of CSE-exposed fibroblasts, we exposed MEFs isolated from MCT4 knockout mouse embryonal fibroblasts (MCT4-KO MEF) and their wild-type (WT) counterparts (WT-MEF) to CSE, in the presence or absence of GSH, and assessed apoptosis and cell death rates (Fig. 3E). MCT4-KO MEFs under baseline conditions have slightly higher apoptosis and cell death levels than WT MEF (1.2 fold, $p = 0.04$). This difference is not significant when unexposed MEFs are treated with GSH (1.2 fold, n.s.). Both genotypes of MEFs have increased apoptosis and cell death rates when treated with CSE. However, MCT4-KO MEF are significantly more sensitive to CSE with 90% higher apoptosis and cell death rates than WT-MEFs. Treatment of CSE-exposed MEFs with GSH greatly reduces cell death and apoptosis in both genotypes. Interestingly, treatment with GSH completely reverses the detrimental effects of CSE on MCT4-KO MEF cell death and apoptosis. Altogether, these data suggests that CSE-induced ROS drives the glycolytic phenotype of fibroblasts, and that MCT4 upregulation is partially necessary for survival of fibroblasts under conditions of CSE exposure.

CSE-fibroblasts reprogram cancer cell metabolism

Metabolic compartmentalization is a common feature in head and neck cancers. Therefore, we wanted to determine whether CSE-exposed fibroblasts with high MCT4 were able to reprogram the metabolism of carcinoma cells towards a more oxidative profile. CAL27 and FaDu cells were co-cultured with CTRL- or CSE-BJ1 for 4 days and the markers of

mitochondrial metabolism MCT1 and TOMM20 were assessed by flow cytometry. Co-culture with CSE-BJ1 increased both MCT1 and TOMM20 expression in CAL27 and FaDu carcinoma cells (Fig. 4A, B). For CAL27, intensity of APC+ staining was quantified by gating the MCT1+ (Fig. 4A, top) and TOMM20+ (Fig. 4A, bottom) cells. For FaDu, percentage of MCT1+ (Fig. 4B, top) and TOMM20+ (Fig. 4B, bottom) cells was quantified. Upregulation of carcinoma cell MCT1 could be visually detected by immunofluorescence staining of CAL27 (Suppl. Fig. 3A) and FaDu (Suppl. Fig. 3B) co-cultures with CSE-BJ1. Moreover, to ensure that the glycolytic phenotype of CSE-BJ1 was preserved after CSE exposure, we assessed the expression of MCT4 in fibroblasts after 4 days in co-culture. CSE-BJ1 maintain MCT4 upregulation after 4 days in co-culture with CAL27 (Fig. 4C) and FaDu (Fig. 4D) cells. We also assessed whether soluble factors secreted by BJ1 could be mediating these effects on carcinoma cells. We treated homotypic cultures of CAL27 and FaDu cells with conditioned media (CM) from CTRL- or CSE-BJ1. CSE-BJ1 CM elicited similar but lessened effects on carcinoma cell MCT1 and TOMM20 in both CAL27 (Suppl. Fig. 3C) and FaDu (Suppl. Fig. 3D) cells. The same effects were seen in transwell co-cultures of MTEC cells with CTRL- or CSE- WT MEFs. WT MEFs exposed to CSE were able to induce MCT1 expression in MTEC cells (Fig. 4E) while MEFs maintained high MCT4 expression 4 days post-CSE-treatment (Fig. 4F).

Altogether, our results show that the CSE-induced metabolic reprogramming of fibroblasts is sufficient to trigger a switch towards oxidative metabolism in carcinoma cells, and these effects are at least in part mediated by soluble factors.

Co-culture with CSE-fibroblasts increases features of tumor aggressiveness

Tumor aggressiveness is defined both by the intrinsic hallmarks of cancer cells and by the cancer-promoting effects of the surrounding stroma. To determine whether the reprogramming of fibroblasts following CSE exposure would produce changes in carcinoma cell aggressiveness, early and late apoptosis and cell death rates were quantified in CAL27 and FaDu cells after 4 days in co-culture with CTRL- or CSE-BJ1. Flow cytometry assessment of AnnV and PI staining showed that co-culture with CSE-BJ1 led to less carcinoma cell death and apoptosis in both CAL27 and FaDu cells (Fig. 5A), with a 50% and 60% decrease, respectively, from co-cultures with CTRL-BJ1. Figure 5B shows the contour plots from three representative samples of each group. Note how in the co-cultures of CAL27 and FaDu cells with CSE-BJ1 there is a reduction in the cell population in the first (Q1), second (Q2) and third quadrants (Q3), corresponding to the dead cells (Q1) and late- and early-apoptotic (Q2+Q3) carcinoma cells.

Cell migration is another common feature of cancer aggressiveness. We assessed the migratory abilities of CAL27 and FaDu cells in response to CTRL- and CSE-BJ1 stimuli with a transwell assay. Carcinoma cells were seeded on top of the porous membrane in the upper chamber of the insert, and CTRL- and CSE-BJ1 were seeded on the bottom chamber. Crystal violet staining of the insert membranes revealed that CSE-BJ1 increased carcinoma cell migration through the pores by 20% in CAL27 and 50% in FaDu cells (Fig. 5C), compared to CTRL-BJ1.

Enhanced replicative capacity is another hallmark of cancer aggressiveness. We assessed proliferation rates in carcinoma cells in co-culture with CTRL- and CSE-BJ1. No differences were seen in cancer cell proliferation between the two types of co-culture in either CAL27 or FaDu cells (Suppl. Fig. 4).

Macrophages constitute a large proportion of the tumor stroma and are associated with aggressive disease and poor prognosis in a variety of human cancers. We studied whether CSE-fibroblasts were able to induce the recruitment of macrophages. We assessed the mRNA levels of the cytokine CCL2, involved in recruitment of monocytes, in WT and MCT4-KO MEFs unexposed or exposed to CSE. Both types of MEFs upregulated CCL2 expression in response to CSE, however WT-MEF did it to a greater extent compared to MCT4-KO MEFs (Fig. 5D). Next, we determined the effects of CTRL- and CSE- WT MEF on the migration capabilities of the mouse macrophage cell line RAW 264.7 by a transwell assay. CSE-exposed MEFs increased the migration of RAW 264.7 cells compared to CTRL-MEFs (Fig. 5E). We were also interested in determining the effects of direct CS-exposure to macrophages on MCT4 expression. MCT4 protein level was assessed by flow cytometry in RAW 267.4 after a 24-hour treatment with 5% CSE or CTRL media. MCT4 was highly upregulated in the macrophages exposed to CSE (Fig. 5F), indicating that the metabolic effects of CSE are not limited to fibroblasts and could be broadened to other cells within the stroma.

Co-injection of carcinoma cells with CSE-fibroblasts increases tumor growth in vivo

To assess whether CSE-fibroblasts would have any effect on carcinoma cell growth in vivo, either CAL27 or FaDu cells were co-injected with CTRL- or CSE-BJ1 into the flanks of nude mice. Tumor size was followed and at day 24 mice were sacrificed and tumors harvested. Tumor growth curves show that co-injection with CSE-BJ1 increased tumor growth in both CAL27 (Suppl. Fig. 5A) and FaDu (Suppl. Fig. 5B) xenografts. Growth differences were significant as early as day 14, which was the first time point when tumor volumes could be measured. We collected tumors at two different time-points for purposes of performing different types of studies, as specified below. At the early time-point, tumor weights were already significantly different between CTRL- and CSE-BJ1 co-injections in both CAL27 (Suppl. Fig. 5C) and FaDu (Suppl. Fig. 5D) tumors. At the endpoint, xenografts generated from co-injections of carcinoma cells with CSE-BJ1 were larger than co-injections with CTRL-BJ1 (Fig. 6A). The volume of CAL27 + CSE-BJ1 xenografts were 2.1 fold (Fig. 6B), and the FaDu + CSE-BJ1 xenografts were 4.7 fold (Fig. 6C) larger than their respective controls.

As we had seen differences in cancer apoptosis and cell death in co-culture studies, we evaluated apoptosis rates in the tumors at the early time-point, when both groups of tumors were actively growing. TUNEL staining revealed decreased cancer cell apoptosis rates in the CSE-BJ1 co-injections in both CAL27 and FaDu xenografts (Fig. 6D, E).

As studies show that CSE induces a pro-inflammatory state in fibroblasts, and our in vitro work demonstrates that CSE-fibroblasts promote macrophage recruitment, we assessed the inflammatory infiltrates in the tumors at the end-point. We performed IHC staining for the leucocyte marker CD45, and CD68, a marker of macrophages and other mononuclear

phagocytes on frozen tumor sections. Xenografts from CAL27 co-injected with CSE-fibroblasts had more CD45+ and CD68+ tumor infiltration than the control co-injection xenografts (Fig. 6F). Quantification of the IHC staining revealed a 4- and 2.1-fold increase in the percentage area invaded by CD45+ and CD68+ cells, respectively (Fig. 6G). FaDu xenografts had high intratumoral and intertumoral variability in macrophage infiltration, and quantification of the IHC staining showed no significant differences in the percentage of area invaded by CD45+ or CD68+ cells between CSE and CTRL groups (Suppl. Fig. 5. E, F).

CSE-induced MCT4 in fibroblasts drives tumor growth

Finally, we wanted to investigate whether stromal MCT4 expression is a driver of the more aggressive growth in tumors observed when cancer cells were co-injected with CSE-fibroblasts. We generated an allograft model by co-injecting MTEC cells with WT MEFs or MCT4-KO MEFs into the flanks of C57BL6 mice. No significant differences in tumor volume and weight were observed between co-injections of MTEC with control WT MEFs and control MCT4-KO MEFs at baseline (Fig. 7A). However, when using MEFs that had been treated with CSE, allografts generated from the co-injection with CSE WT MEF had larger volumes and weight than co-injections with CSE MCT4-KO MEFs (Fig. 7B).

High MCT4 expression is associated with an immune-poor or fibroblast-rich tumor stroma

HNSCC samples from 36 subjects were stained for MCT4 to better understand its relationship with type of stromal infiltrate (immune-rich versus immune-poor), tobacco use and HPV status. The mean age of the subjects was 64 with a range of 41 to 85 and 28 subjects were male and 8 were female. Supplementary table 1 summarizes the subject's baseline characteristics. High stromal MCT4 expression was associated with the presence of immune-poor stroma ($p<0.015$) (Supplementary Table 2). The predominant stromal cell type in all cases of immune-poor stroma were fibroblasts. HPV+ disease was associated with an immune-rich stroma ($p<0.045$), which is consistent with HPV+ disease arising in the lymphoid tissue of the base of tongue and tonsil. However, tobacco use was not associated with an immune-poor stroma. Also, no statistically significant differences were found in stromal MCT4 expression based on tobacco use or HPV status.

Discussion

Cigarette smoke causes many changes in the microenvironment of head and neck carcinomas. Here, we show that cigarette smoke induces phenotypic changes, including metabolic reprogramming, in fibroblasts, and that these altered fibroblasts are sufficient to reprogram the overall metabolism of HNSCC and induce its aggressiveness *in vitro* and *in vivo*. Moreover, we demonstrate that stromal monocarboxylate transporter MCT4 drives cancer aggressiveness in the context of cigarette smoke and describe the aryl hydrocarbon receptor (AhR) pathway as a novel pathway regulating the expression of MCT4.

The tumor stroma supports cancer cells and, for example, CAFs promote proliferation, migration, invasion, and resistance to anti-cancer drugs in a wide array of cancers, including HNSCC[37]. CAFs phenotypically differ from normal fibroblasts since they have increased

remodeling of the extracellular matrix and increased levels of soluble factors and cytokines, which drive a host of effects on carcinoma cells[38]. CAFs also have a reprogrammed metabolism with high glycolytic flux, autophagy and senescence, which are cellular processes that provide a nutrient-rich environment for cancer cells[39]. Metabolically reprogrammed CAFs have been identified in the tumor stroma of HNSCC and have been shown to promote malignant progression[9, 40, 41]. Here, we demonstrate that cigarette smoke metabolically reprograms fibroblasts. CSE exposure increases glycolysis rates in fibroblasts, as seen by upregulation of MCT4 and increases secretion of lactate, as well as inducing senescence. Generation of ROS drives glycolysis and senescence[35, 42] and the current study demonstrates that oxidative stress is a mechanism by which CSE exerts these effects on fibroblasts.

MCT4 is a marker of tumor-associated fibroblasts in a number of cancers, including HNSCC, and is not present in the normal fibroblasts within the adjacent tissue[9]. An MCT4-high stroma may be able to promote transformation by oxidative stress and lactate production. Increased MCT4 expression in the tumor stroma has been associated with decreased overall survival or decreased disease-free survival in several human malignancies[43]. In HNSCC, MCT4 expression in CAFs is associated with higher tumor stage[9] and development of invasive HNSCC in a chemical carcinogenesis model[36]. Our cohort of patients revealed that tumors with a stroma rich in CAFs, as opposed to a stroma rich in immune cells, is associated with high stromal MCT4 expression. In addition, high stromal expression of the carbonic anhydrase IX (CA IX), another marker of oxidative stress and glycolysis, is associated with a poor prognosis in HNSCC[44]. There is an interest in developing therapies against CAFs or the elements participating in the cross-talk between stromal and cancer cells[37]. Here we report ways to modulate fibroblast MCT4 in order to revert the CAF phenotype induced by cigarette smoke. The AhR pathway regulates inflammatory responses[29] and protects fibroblasts from CSE-induced oxidative stress[26–28]. Stimulation of the AhR with the agonist L-KYN decreased the pro-inflammatory transcription factor NF-κB, consistent with the anti-inflammatory role of AhR, at the same time that it downregulated MCT4 expression. However, L-KYN was not able to promote viability of fibroblasts exposed to smoke. Conversely, the antagonist α-NF increased both NF-κB and MCT4 expression, and had an additive effect to cigarette smoke. This is the first publication demonstrating that signaling through the AhR modulates MCT4 expression. Additionally, we studied the effects of antioxidants in our model. Treatment with glutathione abrogated the effects of CSE on ROS levels, MCT4 expression, and lactate secretion in fibroblasts. Also, fibroblasts lacking MCT4 had increased rates of CSE-induced apoptosis and cell death compared to MCT4-expressing fibroblasts, an effect abolished by glutathione treatment. Altogether, our data demonstrates that oxidative stress generated by CSE exposure is a main driver of MCT4 upregulation in fibroblasts, and that MCT4 expression is necessary for fibroblast survival under these conditions.

Cancer cells reprogram stromal cells to derive nutrients, establishing a metabolic cooperation that favors tumor progression[45]. The co-existence of reprogrammed CAFs with high glycolytic metabolism and proliferative cancer cells with high mitochondrial oxidative metabolism is known as “two-compartment tumor metabolism”. Metabolic compartmentalization with high stromal MCT4 and/or high cancer cell MCT1 and

TOMM20, markers of mitochondrial metabolism, occurs in HNSCC[9]. Co-culture models *in vitro* and co-injection models *in vivo* are useful to study the influence of the stroma on carcinoma cells[7, 11, 41]. In breast cancer, a co-culture model of fibroblasts and human breast adenocarcinoma cells showed that the lactate released by fibroblasts induces mitochondrial biogenesis in adjacent carcinoma cells[46]. Here we saw that carcinoma cells co-cultured with CSE-fibroblasts upregulated MCT1 and TOMM20 expression, compared to carcinoma cells co-cultured with unexposed fibroblasts. Moreover, culture of carcinoma cells with conditioned media (CM) from CSE-fibroblasts also induced MCT1 and TOMM20 expression, compared to CM from CTRL-fibroblasts. These data suggests that increased stromal MCT4 and lactate production, together with soluble factors, are sufficient to induce the metabolic reprograming of carcinoma cells.

When we studied the effects of reprogrammed fibroblasts on carcinoma cell aggressiveness we found that co-cultures of carcinoma cells with CSE-exposed fibroblasts greatly reduced apoptosis and cell death rates in the carcinoma compartment. Co-injection of carcinoma cells with CSE-exposed fibroblasts generated larger tumors than co-injection with unexposed fibroblasts. It is well described that tumor associated fibroblasts enhance features of aggressiveness in HNSCC cells[38], however we are the first to show that a microenvironment exposed to CS may be further permissive for HNSCC progression. We also demonstrated that MCT4 upregulation in CS-fibroblasts is an important driver of this effect. Co-injection of syngeneic carcinoma cells with MCT4-KO MEFs exposed to CS generated smaller tumors than co-injections with CS-exposed WT MEFs. No significant difference was observed in the co-injections with unexposed WT and MCT4-KO MEFs, which can be explained by the low basal MCT4 levels in WT MEFs, resembling those of an MCT4-KO MEF. When WT MEFs are stimulated with CS, MCT4 levels rise, and a differential effect versus the MCT4-KO MEFs can be seen. Future studies will need to confirm that the difference in growth is due to low baseline levels of MCT4. We demonstrate that CS-reprogrammed fibroblasts are capable of switching cancer cell metabolism toward a more oxidative metabolism and this metabolic reprogramming in carcinoma cells may be also involved in the promotion of cancer cell aggressiveness. Further studies will need to be performed to assess the effects of mitochondrial inhibitory drugs on tumor growth. HMGB1 arises as another candidate to mediate the cancer-promoting effects of CSE-exposed stroma. HMGB1 is a nuclear factor that can be released from the cell in response to oxidative stress[47]. In our model, CS exposure decreases nuclear HMGB1, presumably releasing it to the extracellular media. Extracellular HMGB1 plays signaling functions through its RAGE receptor that have been shown to promote features of aggressiveness in HNSCC among other cancers[48–50]. Moreover, HMGB1 acts also as a pro-inflammatory cytokine. Altogether, these results demonstrate that CS-induced reprogramming of fibroblasts creates a more favorable tumor microenvironment that induces a metabolic switch in carcinoma cells and promotes their aggressiveness.

HNSCC has abundant immune infiltration[51]. CD68, a macrophage marker, is abundantly expressed in HNSCC tumor tissue, as opposed to normal tissue, and correlates with aggressive behavior, lymph node metastasis, increased incidence of extracapsular spread, and overall worse survival[52–54]. We determined the effects of fibroblast CSE exposure on macrophage recruitment. CSE-exposed fibroblasts have increased levels of the chemokine

CCL2 and are capable of inducing migration of macrophages *in vitro*. Moreover, we assessed the expression of the inflammatory markers CD45, which is a pan-leukocyte marker, and CD68 in our tumors. Despite being and immunocompromised host, nude mice have an intact innate immune system with functional macrophages. Tumors generated from the co-injection with CS-fibroblasts had higher expression of CD45 and CD68, predominantly within the stroma, compared to co-injections with CTRL-fibroblasts. Our data fits with other studies that show that exposure of mice to CSE induces macrophage recruitment in lung tissues and lung tumors, and that these macrophages are polarized to a pro-tumorigenic phenotype[55, 56]. In HNSCC, macrophages promote cell migration, invasion and lymph node metastasis in *in vitro* and *in vivo* models, and are associated with worse outcome in patients[53, 57, 58]. Moreover, studies show the correlation between the density of CAFs and TAMs with poor outcome in HNSCC[59, 60]. Furthermore, one study reported that protumorigenic macrophage polarization is promoted in HNSCC tumors with high lactic acid concentrations[61]. Interestingly, CS-fibroblasts in our model secrete much higher lactate than CTRL-fibroblasts. Our data supports that CS-exposed CAFs with high MCT4 and lactate secretion are capable of recruiting tumor-associated macrophages (TAMs) and promote tumor progression. Future studies will determine the role of MCT4 in the crosstalk between CAFs and TAMs, as well as the contribution of TAMs to tumor growth in the context of a CS-exposed stroma.

Supplementary Material

Refer to Web version on PubMed Central for supplementary material.

Acknowledgements

The National Cancer Institute of the National Institutes of Health under Award Numbers K08 CA175193 (UMO) and 5P30CA056036–17 supported this work. The following SKCC Shared Resources supported by 5P30CA056036–17 were used to conduct this research: Bioimaging Shared Resource, Flow Cytometry Shared Resource, Lab Animal Shared Resource and Translational Pathology Shared Resource. AAO-HNSF Research Award number 411726 (PT) also supported this work.

Abbreviations:

HNSCC	head and neck squamous cell carcinoma
CAF	cancer-associated fibroblast
CS	cigarette smoke
CSE	cigarette smoke extract
CM	conditioned media
MEF	mouse embryonic fibroblast
MCT4	monocarboxylate transporter 4
MCT1	monocarboxylate transporter 1
TOMM20	translocase of the outer mitochondrial membrane 20

pRB	phospho-retinoblastoma
β-gal	β-galactosidase
OXPHOS	oxidative phosphorylation
ROS	reactive oxygen species
NAC	N-acetyl cysteine
GSH	glutathione
AhR	aryl hydrocarbon receptor
L-KYN	L-kynurenine
α-NF	α-naphthoflavone
AnnV	annexin-V
PI	propidium iodide
GFP	green fluorescent protein

References

1. Siegel RL, Miller KD, Jemal A. Cancer statistics, 2016. CA Cancer J Clin. 2016;66: 7–30. [PubMed: 26742998]
2. Hatcher JL, Sterba KR, Tooze JA, et al. Tobacco use and surgical outcomes in patients with head and neck cancer. Head Neck. 2016;38: 700–706. [PubMed: 25521527]
3. Chen AM, Chen LM, Vaughan A, et al. Tobacco smoking during radiation therapy for head-and-neck cancer is associated with unfavorable outcome. Int J Radiat Oncol Biol Phys. 2011;79: 414–419. [PubMed: 20399030]
4. Jethwa AR, Khariwala SS. Tobacco-related carcinogenesis in head and neck cancer. Cancer Metastasis Rev. 2017;36: 411–423. [PubMed: 28801840]
5. Curry JM, Sprandio J, Cognetti D, et al. Tumor microenvironment in head and neck squamous cell carcinoma. Semin Oncol. 2014;41: 217–234. [PubMed: 24787294]
6. Kansy BA, Dissmann PA, Hemeda H, et al. The bidirectional tumor--mesenchymal stromal cell interaction promotes the progression of head and neck cancer. Stem Cell Res Ther. 2014;5: 95. [PubMed: 25115189]
7. Wheeler SE, Shi H, Lin F, et al. Enhancement of head and neck squamous cell carcinoma proliferation, invasion, and metastasis by tumor-associated fibroblasts in preclinical models. Head Neck. 2014;36: 385–392. [PubMed: 23728942]
8. Puram SV, Tirosh I, Parikh AS, et al. Single-Cell Transcriptomic Analysis of Primary and Metastatic Tumor Ecosystems in Head and Neck Cancer. Cell. 2017;171: 1611–1624 e1624. [PubMed: 29198524]
9. Curry JM, Tuluc M, Whitaker-Menezes D, et al. Cancer metabolism, stemness and tumor recurrence: MCT1 and MCT4 are functional biomarkers of metabolic symbiosis in head and neck cancer. Cell Cycle. 2013;12: 1371–1384. [PubMed: 23574725]
10. Curry J, Johnson J, Tassone P, et al. Metformin effects on head and neck squamous carcinoma microenvironment: Window of opportunity trial. Laryngoscope. 2017;127: 1808–1815. [PubMed: 28185288]
11. Tassone P, Domingo-Vidal M, Whitaker-Menezes D, et al. Metformin Effects on Metabolic Coupling and Tumor Growth in Oral Cavity Squamous Cell Carcinoma Coinjection Xenografts. Otolaryngol Head Neck Surg. 2018;158: 867–877. [PubMed: 29232177]

12. Verma A, Rich LJ, Vincent-Chong VK, Seshadri M. Visualizing the effects of metformin on tumor growth, vascularity, and metabolism in head and neck cancer. J Oral Pathol Med. 2018;47: 484–491. [PubMed: 29573032]
13. Nyunoya T, Monick MM, Klingelhutz A, Yarovinsky TO, Cagley JR, Hunninghake GW. Cigarette smoke induces cellular senescence. Am J Respir Cell Mol Biol. 2006;35: 681–688. [PubMed: 16840774]
14. Carnevali S, Petruzzelli S, Longoni B, et al. Cigarette smoke extract induces oxidative stress and apoptosis in human lung fibroblasts. Am J Physiol Lung Cell Mol Physiol. 2003;284: L955–963. [PubMed: 12547733]
15. Rennard SI, Togo S, Holz O. Cigarette smoke inhibits alveolar repair: a mechanism for the development of emphysema. Proc Am Thorac Soc. 2006;3: 703–708. [PubMed: 17065377]
16. Semlali A, Chakir J, Rouabhia M. Effects of whole cigarette smoke on human gingival fibroblast adhesion, growth, and migration. J Toxicol Environ Health A. 2011;74: 848–862. [PubMed: 21598170]
17. Colombo G, Dalle-Donne I, Orioli M, et al. Oxidative damage in human gingival fibroblasts exposed to cigarette smoke. Free Radic Biol Med. 2012;52: 1584–1596. [PubMed: 22387198]
18. Yang GY, Zhang CL, Liu XC, Qian G, Deng DQ. Effects of cigarette smoke extracts on the growth and senescence of skin fibroblasts in vitro. Int J Biol Sci. 2013;9: 613–623. [PubMed: 23847443]
19. Salem AF, Al-Zoubi MS, Whitaker-Menezes D, et al. Cigarette smoke metabolically promotes cancer, via autophagy and premature aging in the host stromal microenvironment. Cell Cycle. 2013;12: 818–825. [PubMed: 23388463]
20. Sato E, Koyama S, Takamizawa A, et al. Smoke extract stimulates lung fibroblasts to release neutrophil and monocyte chemotactic activities. Am J Physiol. 1999;277: L1149–1157. [PubMed: 10600885]
21. Martey CA, Pollock SJ, Turner CK, et al. Cigarette smoke induces cyclooxygenase-2 and microsomal prostaglandin E2 synthase in human lung fibroblasts: implications for lung inflammation and cancer. Am J Physiol Lung Cell Mol Physiol. 2004;287: L981–991. [PubMed: 15234907]
22. D'Anna C, Cigna D, Costanzo G, et al. Cigarette smoke alters cell cycle and induces inflammation in lung fibroblasts. Life Sci. 2015;126: 10–18. [PubMed: 25637683]
23. Moldeus P, Berggren M, Grafstrom R. N-acetylcysteine protection against the toxicity of cigarette smoke and cigarette smoke condensates in various tissues and cells in vitro. Eur J Respir Dis Suppl. 1985;139: 123–129. [PubMed: 3862605]
24. Kim H, Liu X, Kobayashi T, et al. Reversible cigarette smoke extract-induced DNA damage in human lung fibroblasts. Am J Respir Cell Mol Biol. 2004;31: 483–490. [PubMed: 15256382]
25. Ishii T, Matsuse T, Igarashi H, Masuda M, Teramoto S, Ouchi Y. Tobacco smoke reduces viability in human lung fibroblasts: protective effect of glutathione S-transferase P1. Am J Physiol Lung Cell Mol Physiol. 2001;280: L1189–1195. [PubMed: 11350797]
26. Sarill M, Zago M, Sheridan JA, et al. The aryl hydrocarbon receptor suppresses cigarette-smoke-induced oxidative stress in association with dioxin response element (DRE)-independent regulation of sulfiredoxin 1. Free Radic Biol Med. 2015;89: 342–357. [PubMed: 26408075]
27. Iu M, Zago M, Rico de Souza A, et al. RelB attenuates cigarette smoke extract-induced apoptosis in association with transcriptional regulation of the aryl hydrocarbon receptor. Free Radic Biol Med. 2017;108: 19–31. [PubMed: 28254546]
28. Rico de Souza A, Zago M, Pollock SJ, Sime PJ, Phipps RP, Baglole CJ. Genetic ablation of the aryl hydrocarbon receptor causes cigarette smoke-induced mitochondrial dysfunction and apoptosis. J Biol Chem. 2011;286: 43214–43228. [PubMed: 21984831]
29. Baglole CJ, Maggirwar SB, Gasiewicz TA, Thatcher TH, Phipps RP, Sime PJ. The aryl hydrocarbon receptor attenuates tobacco smoke-induced cyclooxygenase-2 and prostaglandin production in lung fibroblasts through regulation of the NF-kappaB family member RelB. J Biol Chem. 2008;283: 28944–28957. [PubMed: 18697742]
30. Pal A, Melling G, Hinsley EE, et al. Cigarette smoke condensate promotes pro-tumourigenic stromal-epithelial interactions by suppressing miR-145. J Oral Pathol Med. 2013;42: 309–314. [PubMed: 23173553]

31. Nyunoya T, Monick MM, Klingelhutz AL, et al. Cigarette smoke induces cellular senescence via Werner's syndrome protein down-regulation. Am J Respir Crit Care Med. 2009;179: 279–287. [PubMed: 19011155]
32. Monick MM, Powers LS, Walters K, et al. Identification of an autophagy defect in smokers' alveolar macrophages. J Immunol. 2010;185: 5425–5435. [PubMed: 20921532]
33. Kim SY, Lee JH, Huh JW, et al. Cigarette smoke induces Akt protein degradation by the ubiquitin-proteasome system. J Biol Chem. 2011;286: 31932–31943. [PubMed: 21778238]
34. Gross TJ, Powers LS, Boudreau RL, et al. A microRNA processing defect in smokers' macrophages is linked to SUMOylation of the endonuclease DICER. J Biol Chem. 2014;289: 12823–12834. [PubMed: 24668803]
35. Martinez-Outschoorn UE, Curry JM, Ko YH, et al. Oncogenes and inflammation rewire host energy metabolism in the tumor microenvironment: RAS and NFkappaB target stromal MCT4. Cell Cycle. 2013;12: 2580–2597. [PubMed: 23860378]
36. Bisetto S, Whitaker-Menezes D, Wilski NA, et al. Monocarboxylate Transporter 4 (MCT4) Knockout Mice Have Attenuated 4NQO Induced Carcinogenesis; A Role for MCT4 in Driving Oral Squamous Cell Cancer. Front Oncol. 2018;8: 324. [PubMed: 30211114]
37. Schmitz S, Machiels JP. Targeting the Tumor Environment in Squamous Cell Carcinoma of the Head and Neck. Curr Treat Options Oncol. 2016;17: 37. [PubMed: 27262711]
38. Liao Z, Tan ZW, Zhu P, Tan NS. Cancer-associated fibroblasts in tumor microenvironment - Accomplices in tumor malignancy. Cell Immunol. 2018.
39. Avagliano A, Granato G, Ruocco MR, et al. Metabolic Reprogramming of Cancer Associated Fibroblasts: The Slavery of Stromal Fibroblasts. Biomed Res Int. 2018;2018: 6075403. [PubMed: 29967776]
40. Curry J, Tassone P, Gill K, et al. Tumor Metabolism in the Microenvironment of Nodal Metastasis in Oral Squamous Cell Carcinoma. Otolaryngol Head Neck Surg. 2017;157: 798–807. [PubMed: 28608777]
41. New J, Arnold L, Ananth M, et al. Secretory Autophagy in Cancer-Associated Fibroblasts Promotes Head and Neck Cancer Progression and Offers a Novel Therapeutic Target. Cancer Res. 2017;77: 6679–6691. [PubMed: 28972076]
42. Martinez-Outschoorn UE, Balliet RM, Rivadeneira DB, et al. Oxidative stress in cancer associated fibroblasts drives tumor-stroma co-evolution: A new paradigm for understanding tumor metabolism, the field effect and genomic instability in cancer cells. Cell Cycle. 2010;9: 3256–3276. [PubMed: 20814239]
43. Bovenzi CD, Hamilton J, Tassone P, et al. Prognostic Indications of Elevated MCT4 and CD147 across Cancer Types: A Meta-Analysis. Biomed Res Int. 2015;2015: 242437. [PubMed: 26779534]
44. Brockton N, Dort J, Lau H, et al. High stromal carbonic anhydrase IX expression is associated with decreased survival in P16-negative head-and-neck tumors. Int J Radiat Oncol Biol Phys. 2011;80: 249–257. [PubMed: 21300470]
45. Gouirand V, Guillaumond F, Vasseur S. Influence of the Tumor Microenvironment on Cancer Cells Metabolic Reprogramming. Front Oncol. 2018;8: 117. [PubMed: 29725585]
46. Martinez-Outschoorn UE, Pavlides S, Howell A, et al. Stromal-epithelial metabolic coupling in cancer: integrating autophagy and metabolism in the tumor microenvironment. Int J Biochem Cell Biol. 2011;43: 1045–1051. [PubMed: 21300172]
47. Yu Y, Tang D, Kang R. Oxidative stress-mediated HMGB1 biology. Front Physiol. 2015;6: 93. [PubMed: 25904867]
48. Nguyen A, Bhavsar S, Riley E, Caponetti G, Agrawal D. Clinical Value of High Mobility Group Box 1 and the Receptor for Advanced Glycation End-products in Head and Neck Cancer: A Systematic Review. Int Arch Otorhinolaryngol. 2016;20: 382–389. [PubMed: 27746844]
49. Li Y, Wang P, Zhao J, Li H, Liu D, Zhu W. HMGB1 attenuates TGF-beta-induced epithelial-mesenchymal transition of FaDu hypopharyngeal carcinoma cells through regulation of RAGE expression. Mol Cell Biochem. 2017;431: 1–10. [PubMed: 28285361]
50. Di X, He G, Chen H, et al. High-mobility group box 1 protein modulated proliferation and radioresistance in esophageal squamous cell carcinoma. J Gastroenterol Hepatol. 2018.

51. Mandal R, Senbabaoglu Y, Desrichard A, et al. The head and neck cancer immune landscape and its immunotherapeutic implications. JCI Insight. 2016;1: e89829. [PubMed: 27777979]
52. Balermpas P, Rodel F, Liberz R, et al. Head and neck cancer relapse after chemoradiotherapy correlates with CD163+ macrophages in primary tumour and CD11b+ myeloid cells in recurrences. Br J Cancer. 2014;111: 1509–1518. [PubMed: 25093488]
53. Seminerio I, Kindt N, Descamps G, et al. High infiltration of CD68+ macrophages is associated with poor prognoses of head and neck squamous cell carcinoma patients and is influenced by human papillomavirus. Oncotarget. 2018;9: 11046–11059. [PubMed: 29541395]
54. Marcus B, Arenberg D, Lee J, et al. Prognostic factors in oral cavity and oropharyngeal squamous cell carcinoma. Cancer. 2004;101: 2779–2787. [PubMed: 15546137]
55. Oliveira da Silva C, Monte-Alto-Costa A, Renovato-Martins M, et al. Time Course of the Phenotype of Blood and Bone Marrow Monocytes and Macrophages in the Lung after Cigarette Smoke Exposure In Vivo. Int J Mol Sci. 2017;18.
56. Kameyama N, Chubachi S, Hegab AE, et al. Intermittent Exposure to Cigarette Smoke Increases Lung Tumors and the Severity of Emphysema More than Continuous Exposure. Am J Respir Cell Mol Biol. 2018;59: 179–188. [PubMed: 29443539]
57. Tsujikawa T, Yaguchi T, Ohmura G, et al. Autocrine and paracrine loops between cancer cells and macrophages promote lymph node metastasis via CCR4/CCL22 in head and neck squamous cell carcinoma. Int J Cancer. 2013;132: 2755–2766. [PubMed: 23180648]
58. Gao L, Wang FQ, Li HM, et al. CCL2/EGF positive feedback loop between cancer cells and macrophages promotes cell migration and invasion in head and neck squamous cell carcinoma. Oncotarget. 2016;7: 87037–87051. [PubMed: 27888616]
59. Yu Y, Ke L, Lv X, et al. The prognostic significance of carcinoma-associated fibroblasts and tumor-associated macrophages in nasopharyngeal carcinoma. Cancer Manag Res. 2018;10: 1935–1946. [PubMed: 30022852]
60. Fujii N, Shomori K, Shiomi T, et al. Cancer-associated fibroblasts and CD163-positive macrophages in oral squamous cell carcinoma: their clinicopathological and prognostic significance. J Oral Pathol Med. 2012;41: 444–451. [PubMed: 22296275]
61. Ohashi T, Aoki M, Tomita H, et al. M2-like macrophage polarization in high lactic acid-producing head and neck cancer. Cancer Sci. 2017;108: 1128–1134. [PubMed: 28370718]

Implications:

Cigarette smoke shifts cancer-stroma towards glycolysis and induces head and neck cancer aggressiveness with a mitochondrial profile linked by catabolite transporters and oxidative stress.

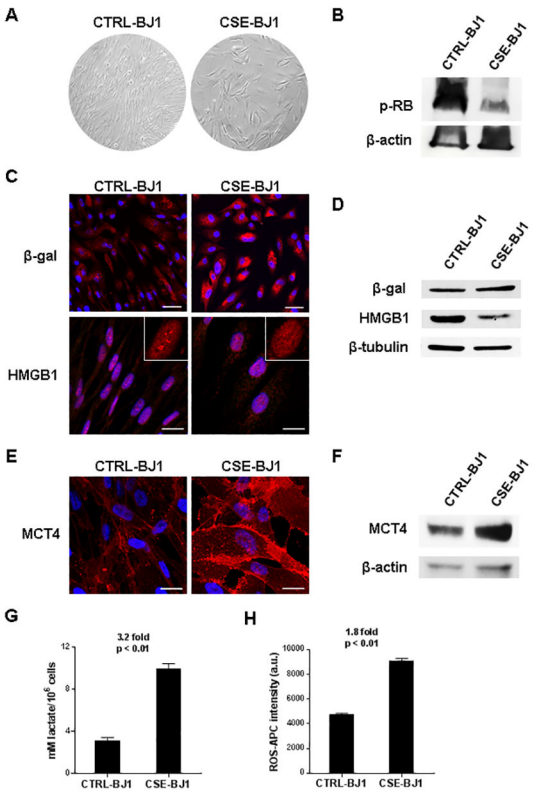

Figure 1.

Cigarette Smoke induces senescence and a metabolic switch towards glycolysis in fibroblasts. BJ1 fibroblasts were cultured in standard or cigarette smoke extract (CSE) media (CTRL-BJ1 and CSE-BJ1, respectively) for 6 days, refreshing the media every 2 days. **A,** Visual assessment of fibroblast density and morphology under the miscroscope at 10X. **B,** Analysis of the proliferation marker p-RB by western blot. **C-D,** Analysis of the markers of senescence β-gal and HMGB1 by immunofluorescence (C) and western blot (D). **E-F,** Analysis of the marker of glycolysis MCT4 by immunofluorescence (E) and western blot (F). In all immunofluorescence staining, β-gal, HMGB1 and MCT4 are shown in red, and nuclei are shown in blue (DAPI). DAPI channel intensity was removed in HMGB1 zoom-ins to appreciate nuclear staining. Confocal microscopy images were acquired at the 40X magnification, with additional 2x zoom for HMGB1 and MCT4. Scale bar: 50 μm (β-gal) or 20 μm (HMGB1 and MCT4). **G,** Assessment of lactate levels in media of CTRL- and CSE-BJ1 by colorimetric assay. **H,** Assessment of intracellular ROS levels of CTRL- and CSE-BJ1 by flow cytometry.

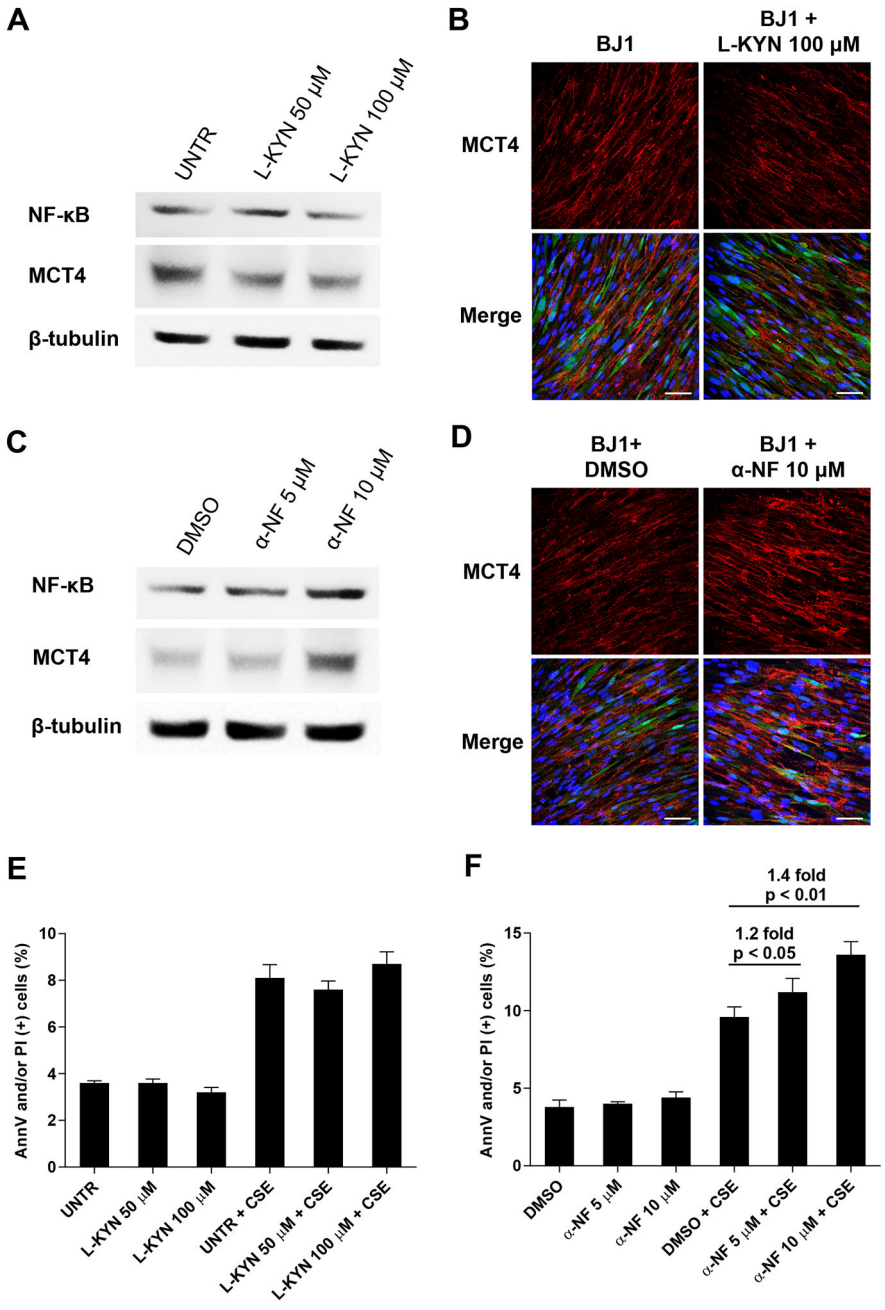

Figure 2.

Signaling through the aryl hydrocarbon receptor (AhR) modulates expression of MCT4 in fibroblasts. BJ1 fibroblasts were cultured in CTRL- and CSE-media and treated with increasing concentrations of the AhR agonist L-kynurenine (L-KYN) or the antagonist α-naphthoflavone (α-NF). **A,** Western blot assessment of MCT4 and NF-κB expression in CTRL-BJ1 untreated or treated with 50 and 100 μM of L-KYN. **B,** Immunofluorescence staining of MCT4 (red) in CTRL-BJ1 untreated or treated with 100 μM L-KYN. Merged images show GFP-expressing BJ1 in green and nuclei stained with DAPI in blue. Scale bar: 50 μm. **C,** Western blot assessment of MCT4 and NF-κB expression in CTRL-BJ1 treated

with 5 and 10 μM of α-NF or vehicle DMSO. **D,** Immunofluorescence staining of MCT4 (red) in CTRL-BJ1 treated with 10 μM α-NF or vehicle DMSO. Merged images show GFP-expressing BJ1 in green and nuclei stained with DAPI in blue. Scale Bar: 50 μm. **E-F,** Apoptosis and cell death percentages assessment of CTRL- and CSE-BJ1 treated with L-KYN (E) or α-NF (F). Apoptosis was detected by annexin V (AnnV) staining and cell death by propidium iodide (PI) staining by flow cytometry.

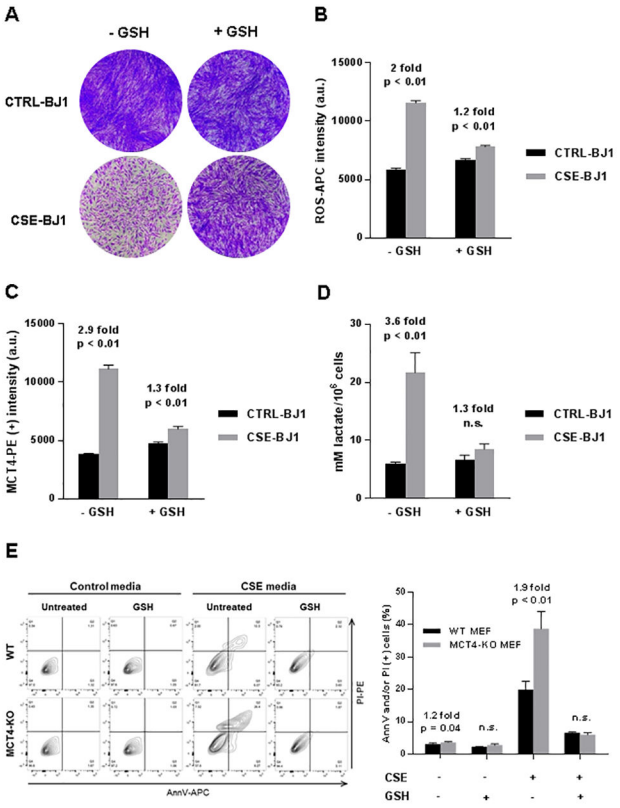

Figure 3.

The antioxidant glutathione abrogates the effects of CSE. Fibroblasts were cultured in CTRL- or CSE-media and treated with 30 μg/ml of liposomal glutathione (GSH). **A,** Crystal violet (CV) staining of CTRL- and CSE-BJ1 untreated or treated with GSH. **B-C,** Assessment of intracellular ROS levels in (B), MCT4 expression (C), and secreted lactate levels (D) in BJ1 fibroblasts, by flow cytometry. **E,** Assessment of cell viability in WT and MCT4-KO MEF exposed to CSE in the presence or absence of GSH. Left, flow cytometry contour plots of representative samples. AnnV staining intensity is represented in the X-axis and PI staining on the Y-axis. Dead cells are found in quadrant 1 (Q1), apoptotic cells in Q2+Q3, and live cells in Q4. Right, quantification of quadrants Q1-Q3 corresponding to apoptotic and dead cells (AnnV and/or PI positive).

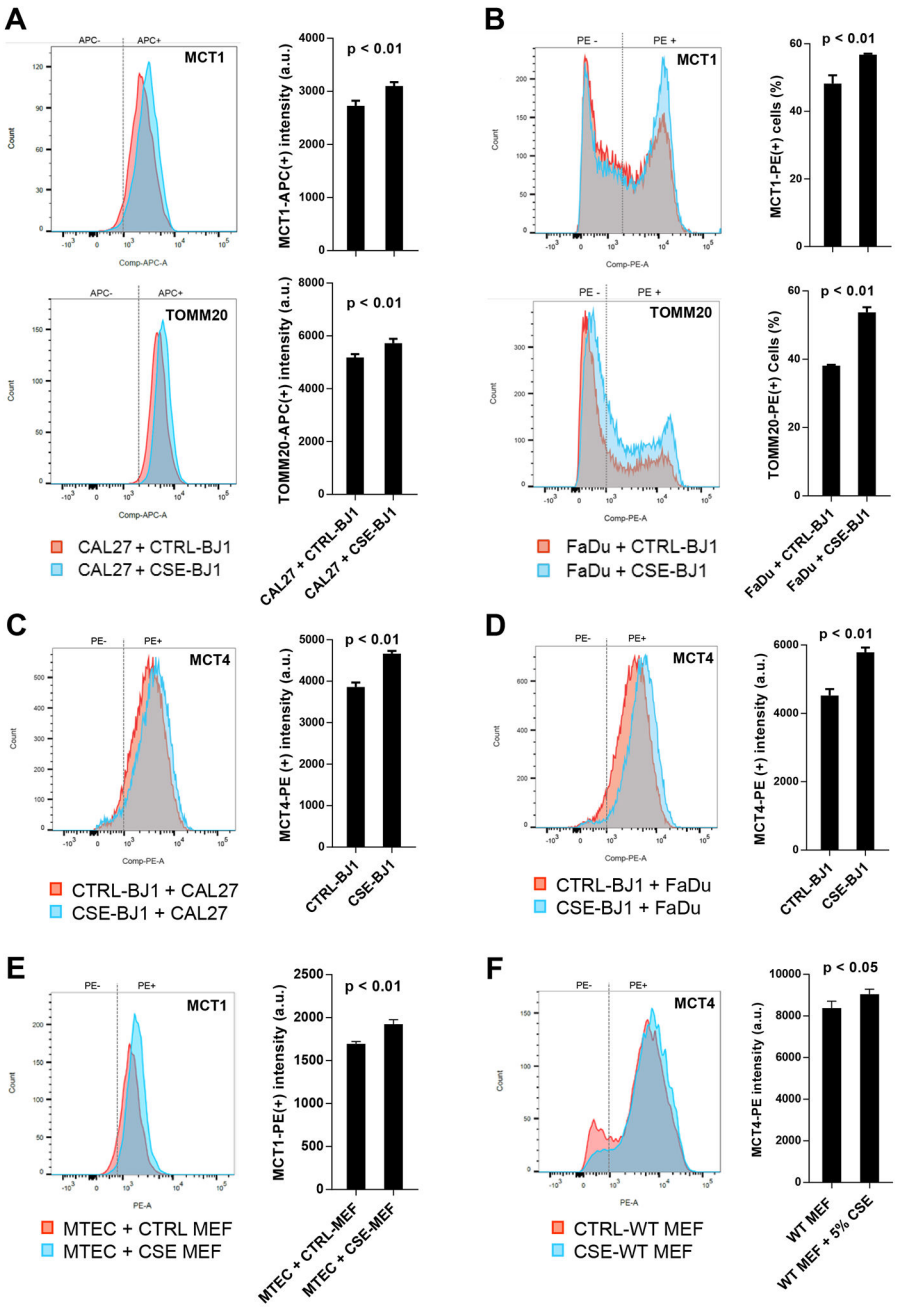

Figure 4.

CSE-fibroblasts induce markers of mitochondrial metabolism on carcinoma cells. **A-D,** CAL27 and FaDu cells were co-cultured with CTRL- or CSE-BJ1 and cancer cell MCT1 and TOMM20, and fibroblast MCT4 expression was assessed by flow cytometry. **A,** Flow cytometry plots and quantification of MCT1 (top) and TOMM20 (bottom) staining intensity in CAL27 co-cultures. **B,** Flow cytometry plots and quantification of percentage of cells expressing MCT1 (top) and TOMM20 (bottom) in FaDu co-cultures. **C-D,** MCT4 expression in CTRL- and CSE-BJ1 after 4 days in co-culture with CAL27 (C) and FaDu (D) cells. **E-F,** MTEC cells were co-cultured with WT MEF previously exposed to CTRL or

CSE media, and cancer cell MCT1 and fibroblast MCT4 expression were assessed by flow cytometry. **E,** Flow cytometry plots and quantification of MCT1 staining intensity in MTEC cells. **F,** Flow cytometry plots and quantification of MCT4 staining intensity in WT MEFs 4 days post-CTRL or CSE treatment. For all markers, staining intensity was gated into APC- and APC+ or PE- and PE+ based on the signal into the APC and PE channels, respectively, emitted by the unstained control. Only APC+ and PE+ populations were used for quantification.

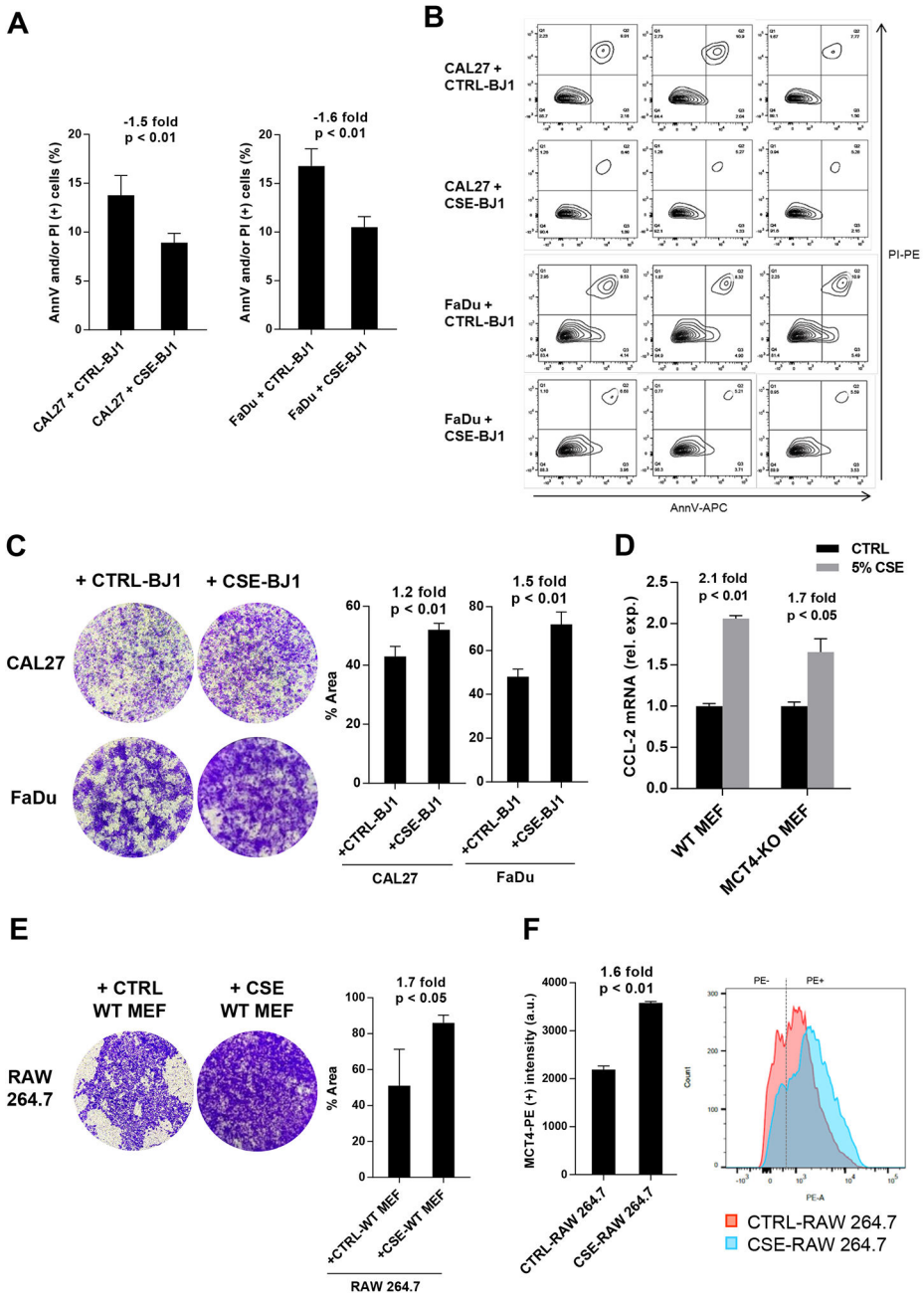

Figure 5.

CSE-exposed fibroblasts increase features of tumor aggressiveness. **A-B,** CAL27 and FaDu cells were co-cultured with CTRL- or CSE-BJ1 and apoptosis and cell death rates were assessed by flow cytometry and cell migration by a transwell assay. **A,** Quantification of quadrants Q1-Q3 (from panel C) corresponding to apoptotic and dead CAL27 and FaDu carcinoma cells (AnnV and/or PI positive). **B,** Contour plots of AnnV (X-axis) and PI (Y-axis) staining in CAL27 and FaDu cells co-cultured with fibroblasts. Dead cells are found in quadrant 1 (Q1), apoptotic cells in Q2+Q3, and live cells in Q4. **C,** Assessment of the migratory ability of CAL27 and FaDu carcinoma cells stimulated by CTRL- or CSE-BJ1.

On the left, crystal violet (CV) staining of the cells that migrated through the pores of the membrane; on the right, quantification of the percentage area of the membrane stained by CV. **D-F,** Assessment of the effects of CSE-fibroblasts on immune cell migration. **D,** Quantification of CCL2 mRNA levels in WT and MCT4-KO MEF exposed to CTRL- or CSE-media. **E,** Transwell migration assay with CV staining of RAW 264.7 cells that migrated through the membrane in response to WT MEFs previously exposed to CTRL- or CSE-media. **F,** Flow cytometry plots and quantification of MCT4 staining intensity in RAW 264.7 exposed to CTRL- or CSE-media.

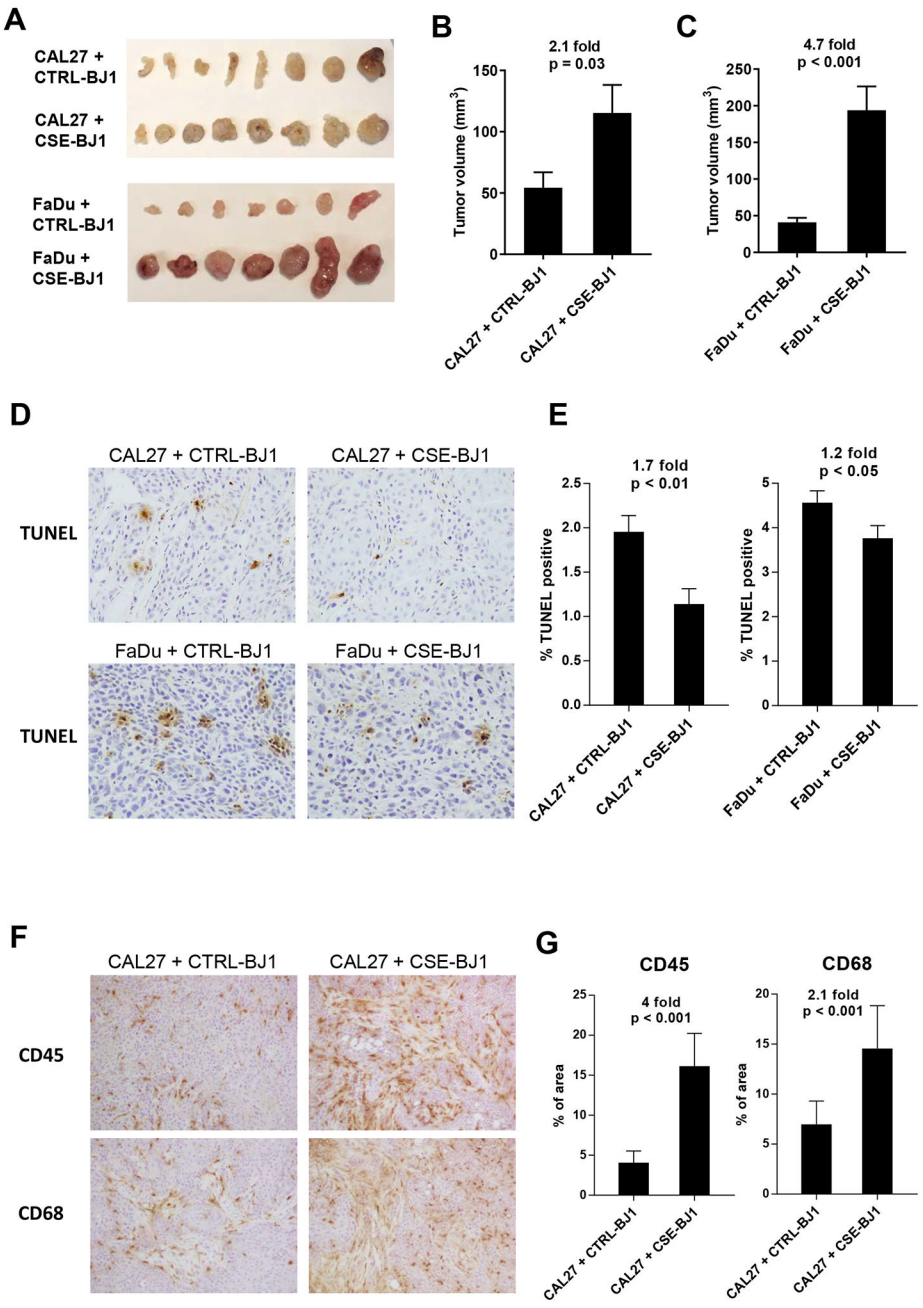

Figure 6.

CSE-exposure in fibroblasts promote tumor growth and inflammation. CAL27 and FaDu cells were co-injected with CTRL- and CSE-BJ1 into the flanks of immunocompromised nude mice **A**, Images of harvested tumor xenografts for gross volume comparison. **B-C**, Volumes of harvested tumor xenografts generated from CAL27 (B) and FaDu (C) and fibroblast co-injections. **D-E,** Apoptosis rates were measured by staining (D) and quantification (E) of TUNEL in CAL27 and FaDu tumor xenografts. **F-G**, IHC assessment of the pan-lymphocyte marker, CD45, and macrophage marker, CD68, on CAL27 tumor

samples. Representative areas of CD45 and CD68 infiltration (F) and quantification of percentage of stained area (G) in CAL27 xenografts.

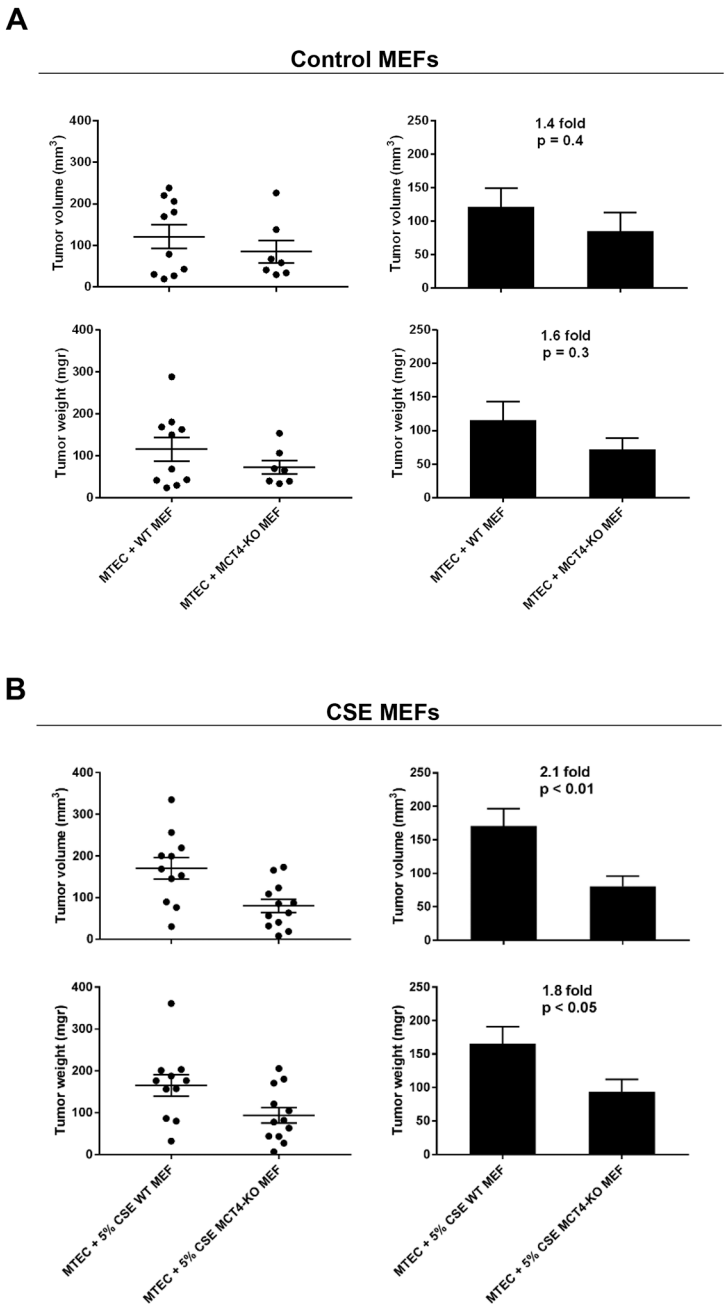

Figure 7.

MCT4 expression in fibroblasts induced by CSE drives tumor growth. MTEC carcinoma cells were co-injected with unexposed or CSE-exposed WT and MCT4-KO MEFs into the flanks of C57BL/6 mice. **A,** Tumor volume (top) and weight (bottom) of harvested allografts generated from the co-injection of MTEC with control MEFs. **B**, Tumor volumes (top) and weights (bottom) of harvested allografts generated from the co-injection of MTEC with CSE-exposed MEFs.

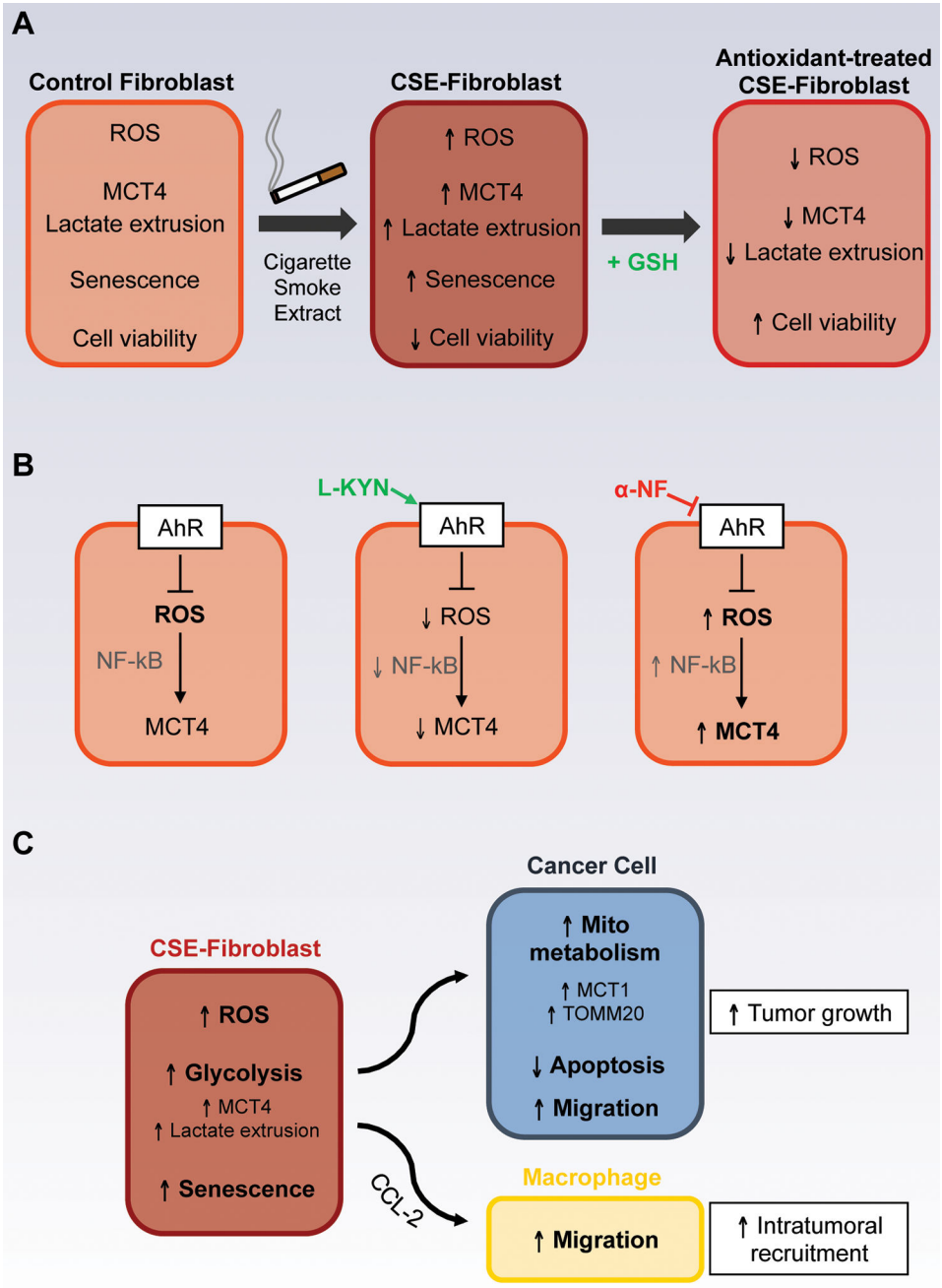

Visual Overview.

Summary diagram of main findings and biological relevance. **A**, Exposure of fibroblasts to cigarette smoke induces ROS generation and a metabolic switch toward glycolysis, as seen by an upregulation of the glycolytic marker MCT4 and the increased secretion of lactate, end-product of glycolysis. Cigarette smoke extract (CSE) also induces cellular senescence and decreases cell viability in fibroblasts. Addition of the antioxidant glutathione (GSH) abrogates the effects of CSE by decreasing ROS levels and reducing MCT4 expression and lactate extrusion. **B**, AhR signaling is able to modulate MCT4 expression. L-KYN is an AhR agonist and reduces the inflammatory state of the cell, as seen by decreased NF-kB

expression, and also MCT4 levels. α-NF is an AhR antagonist and induces both NF-kB and MCT4 expression. **C**, CSE-exposed fibroblasts induce cancer cell aggressiveness both *in vitro* and *in vivo*. Carcinoma cells co-cultured with CSE-fibroblasts expressing high MCT4 levels increase MCT1 expression and mitochondrial metabolism. Moreover, CSE-fibroblasts induce resistance to cell death and facilitate migration of carcinoma cells. Co-injection of carcinoma cells with CSE-fibroblasts promotes tumor growth in an MCT4-dependent manner. CSE-fibroblasts also have effects on macrophages. CSE-exposure induces CCL2 secretion and increases migration of macrophages *in vitro*. Co-injection of carcinoma cells with CSE-fibroblasts promote the recruitment of macrophages into the tumor.